The 4th International Symposium - Supercritical CO_2 Power Cycles
September 9-10, 2014, Pittsburgh, Pennsylvania

RECENT DEVELOPMENTS IN S-CO_2 CYCLE DYNAMIC MODELING AND ANALYSIS AT ANL

Anton Moisseytsev
Principal Nuclear Engineer
Argonne National Laboratory
Argonne, IL USA
amoissey@anl.gov

James J. Sienicki
Senior Nuclear Engineer
Argonne National Laboratory
Argonne, IL USA
sienicki@anl.gov

Anton Moisseytsev is a Principal Computational Nuclear Engineer at Nuclear Engineering Division of Argonne National Laboratory. He has ten years of experience in modeling and simulation of various systems, including design and analysis of the advanced reactors and energy conversion systems, safety analysis of nuclear reactors, and code development for steady-state and transient simulations of nuclear power plants. Anton has been involved in the development of the supercritical carbon dioxide Brayton cycle at Argonne since 2002.

James J. Sienicki is the Manager of the Innovative Systems and Engineering Assessments Section and a Senior Nuclear Engineer in the Nuclear Engineering Division at ANL. He has been leading the development of the supercritical carbon dioxide Brayton cycle at ANL with funding from the U.S. Department of Energy since 2002. He is also involved in the design and analysis of experiments on fundamental phenomena involved in heat exchangers for supercritical CO_2 cycles.

ABSTRACT

The paper provides an update on recent (since the last S-CO_2 Symposium in 2011) analyses of the S-CO_2 Brayton cycle at ANL. The majority of these new analyses have been focused on continuation of development of the S-CO_2 cycle control strategy with the ANL Plant Dynamics Code (PDC) as well as on validation of the PDC. Most of the S-CO_2 cycle control analysis at ANL has been done in application of the cycle as an energy converter for Sodium-Cooled Fast Reactors (SFRs). An approach has been developed to couple the PDC to the SAS4A/SASSYS-1 Liquid Metal Reactor Analysis Code System in transient calculations. Analyses have shown that a SFR with a S-CO_2 Brayton cycle power converter can perform load following over the complete range of grid demand from 100 to 0 % nominal. Further analyses have shown that the S-CO_2 Brayton cycle can be used to remove power from the reactor and reject it to the heat sink following disconnection from the electrical grid. Heat removal is possible down to initial decay heat levels of at least as low as 3 % nominal power. This is accomplished by a combination of a new control mechanism of shaft speed control following disconnection from the grid and active control of the reactor power and primary and intermediate sodium pump speeds.

The PDC validation effort is currently focusing on the experimental data obtained at the SNL small-scale integral S-CO_2 loop. The SNL data is used to validate and further improve both the steady-state and transient models of the PDC, including the individual components. Specifics of the loop design, small-scale effects, and operation have presented some challenges for model validation. This includes lack of specific information due to restrictions on component design information, unmeasured significant heat losses in various locations and components, and less than sufficient (from the modeler's point of view) measurements and/or accuracy of the measurements. Much has been learned about the loop and how to overcome the difficulties through modeling approaches. Good agreement with the experimental data is being obtained for both steady-state and transient results, and future model improvements have been identified.

INTRODUCTION

Control of a supercritical carbon dioxide (S-CO_2) Brayton cycle is often perceived as a difficult task. The challenges in the S-CO_2 cycle control originate from the specifics of the cycle conditions and design, such as significant properties variation near the critical point, recompression cycle configuration with two compressors working in parallel, and significant thermal inertia of the large cycle heat exchangers. For these reasons, the majority of the S-CO_2 cycle analysis work at the Argonne National Laboratory (ANL) has been devoted to the development of a control strategy for the cycle.

The analysis presented is this paper has been carried out using the Plant Dynamics Code (PDC) developed at ANL. The Plant Dynamics Code has been developed specifically for the analysis of the S-CO_2 cycle (Moisseytsev and Sienicki, 2006). From the beginning, the focus of PDC development has been on capturing the unique features of the S-CO_2 cycle, such as properties variation, especially near the critical point, and the effect of the CO_2 properties on the design and performance of the cycle components and the entire system. For example, the ideal gas laws commonly used for turbomachinery and heat exchanger analysis (e.g., log-mean temperature approach) are not applicable to the CO_2 cycle and were intentionally not included into the PDC equations. Instead, the code relies on fundamental conservation laws, such as energy, mass, and momentum, and very accurate CO_2 properties calculations. In the PDC, the original Span and Wagner (1996) formulations of CO_2 properties (with up to 42 polynomial terms) are used without any simplifications (although, with optimization for speed) in both the steady-state and dynamic calculations. The PDC has two parts: steady-state and transient, intended for design and transient performance analysis, respectively. Most of the control analysis presented in this paper has been carried out using the transient capabilities of the PDC. In addition to the PDC features described above, there are several code features which are beneficial for control strategy development and analysis. These features include: i) implementation of various control mechanisms with Proportional, Integral, and Differential (PID) user input and limitations on valve speeds, ii) accurate simulation of the CO_2 flow through the valves, including pressure wave propagation with sonic limits and CO_2 properties variation in the valve, iii) possibility to either use detailed four-dimensional turbomachinery maps or direct turbomachinery performance subroutines, iv) calculation of turbine and compressor stall and choke margins on each time strep, and v) support of synchronous and asynchronous generator connection modes to the electrical grid. In addition, coupling the PDC to a reactor analysis code, also described in this paper, allows for analysis of control of the coupled reactor and balance-of-plant (BOP) system.

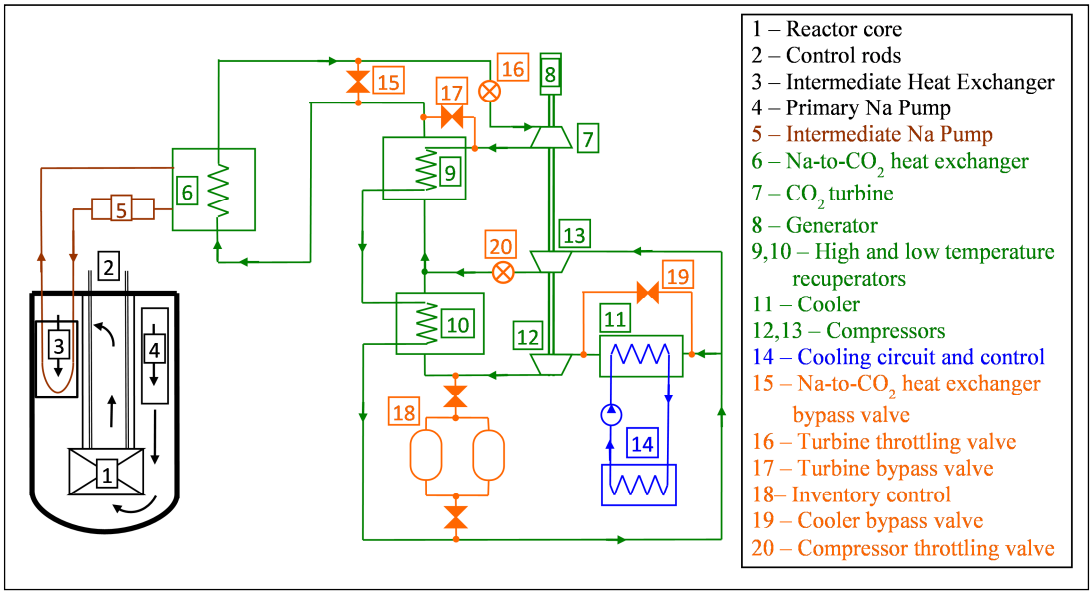

Figure 1. SFR with S-CO_2 Cycle: Layout and Control Mechanisms.

Earlier results of S-CO_2 cycle control with the PDC have been presented at previous S-CO_2 symposia (Moisseytsev, 2007; Moisseytsev and Sienicki, 2009 and 2011a). This paper describes the most recent ANL analysis and results in the field of cycle control and transient simulation. The material presented in this paper covers the progress obtained from the previous S-CO_2 Symposium in 2011. The majority of the results in this paper has been already presented at various conferences. Thus, this paper has been prepared as an update for the current symposium attendees.

Most of the S-CO_2 cycle control analysis carried out at ANL and presented in this paper has been done in application of the cycle as an energy converter for Sodium-Cooled Fast Reactors (SFRs). The analyzed cycle configuration, including the reactor loops, cycle components, and control mechanism, is shown in Figure 1. Although some SFR-specific features of the S-CO_2 cycle control have been identified, the majority of the results and findings presented here would be applicable to other applications and designs of the cycle.

COUPLING OF THE PDC WITH THE SAS4A/SASSYS-1 CODE

In any transient calculation of the S-CO_2 cycle coupled to a reactor, the reactor-side fluid conditions, including temperature, flow rate, and pressure, at the reactor heat exchanger (RHX) need to be defined. In the case of a SFR, the RHX would be an intermediate sodium-to-CO_2 heat exchanger. In earlier SFR cycle analysis, those reactor-side fluid conditions were either provided by a user as tables or were calculated separately (and iteratively) using a separate reactor analysis code (Moisseytsev and Sienicki, 2011b), such as SAS4A/SASSYS-1.

The SAS4A/SASSYS-1 Liquid Metal Reactor Code System (Cahalan et.al., 1994) is the leading capability for modeling liquid-metal cooled reactors (e.g., SFRs) at the system level. The SAS4A/SASSYS-1 code couples reactor dynamics with thermal hydraulics calculations. The SAS4A/SASSYS-1 code incorporates very detailed reactivity feedback models along with comprehensive thermal hydraulic models for the primary, intermediate, and decay heat liquid metal loops. The SAS4A/SASSYS-1 code also supports the modeling of the balance-of-plant. However, this option is currently limited to steam cycles only.

A new coupling approach between the SAS4A/SASSYS-1 and PDC codes was developed to simplify the transient analysis of a SFR with a S-CO_2 cycle. The main goal of the coupling was to implement data transfer between the two codes at each time step (rather than after the entire transient is calculated). In the coupled calculations for a SFR, using the algorithm shown in Figure 2, the SAS4A/SASSYS-1 code calculates the conditions on the reactor side for primary and intermediate coolants, and provides the intermediate sodium conditions at the RHX inlet and its flow rate at each time step. The PDC then uses this input to calculate the transient response of the RHX, including the sodium and CO_2 sides, and the rest of the S-CO_2 cycle conditions during the time step. The RHX-outlet temperature on the sodium side is supplied back to the SAS4A/SASSYS-1 code for the calculations for the next time step.

The coupling was done using an executable file for the SAS4A/SASSYS-1 code, avoiding the need for modification of the SAS4A/SASSYS-1 source code. The coupling approach utilizes the restart capability of SAS4A/SASSYS-1 and allows for data transfer between the two codes at each time step. The approach could also be used to couple the PDC to other system level reactor dynamics codes for other reactor types as well as codes for other S-CO_2 cycle heat sources (e.g., fossil energy, solar power tower). All of the cycle control calculations presented below were carried out using the coupled PDC-SAS4A/SASSYS-1 codes.

DYNAMIC SIMULATION AND CONTROL OF THE S-CO_2 CYCLE

The Plant Dynamics Code has been used extensively for S-CO_2 cycle control strategy development and simulation. In this section, the results of calculations carried out using the coupled PDC-SAS4A/SASSYS-1 code for a 1000 MWt metallic-fueled SFR are presented. The entire system modeled is shown in Figure 1 along with the control mechanisms for the S-CO_2 cycle, including turbine bypass, turbine throttling, inventory, and minimum CO_2 temperature controls. On the reactor side, an autonomous operation strategy is simulated meaning that no deliberate motion of control rods or adjustment of sodium pump speeds is assumed to take place. Instead, the reactor is allowed to adjust its power through the inherent reactivity feedbacks in response to the changing coolant temperatures when heat removal by the S-CO_2 cycle varies in a transient.

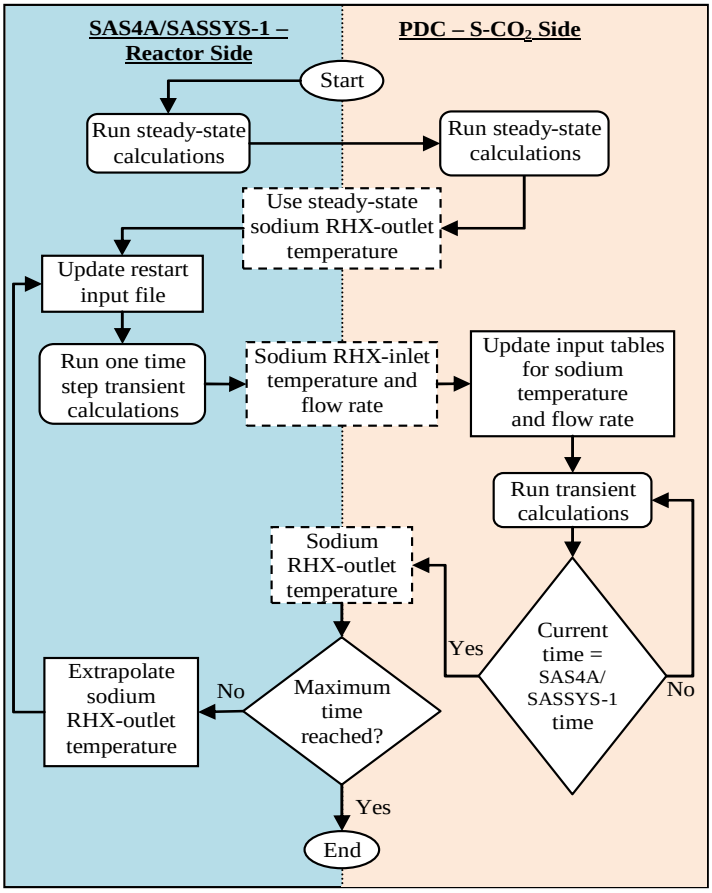

Figure 2. PDC-SAS4A/SASSYS-1 Coupling Approach.

The transient simulated here consists of two parts. First, the cycle's load following capabilities are demonstrated by simulating the plant response to a linear reduction in electrical grid demand. When the grid demand reaches zero, the second stage of the transient is initiated by disconnecting the plant from the grid followed by the transition to the decay heat removal mode.

Load Following and Automatic S-CO_2 Cycle Control

The load following transient is initiated at full power conditions. It is specified that the electrical grid demand decreases linearly from the 100% level to 0% in 20 minutes, i.e. at a 5%/min rate. The automatic control of the S-CO_2 cycle will adjust the generator output in order to match the decreasing grid demand. The S-CO_2 cycle control strategy is summarized in Figure 3; where the control mechanisms employed during load following are shown on the right hand side of the graph. This strategy was previously developed (Moisseytsev and Sienicki, 2006, 2008 and 2010) for the cycle using the Plant Dynamics Code in order to achieve stable and the most efficient operation at partial loads.

The results of the transient simulation are presented in Figure 4, which shows the combined results of the two stages of the transient that are separated at the 1200 seconds mark when the reactor is disconnected from the grid. The two stages are separated with vertical lines on each plot in Figure 4.

As demonstrated in Figure 4, the reducing electrical grid demand is very closely matched by the net generator output (Figure 4(a)). This is achieved by automatic control of the S-CO_2 cycle which simulates an action of the control valves shown in Figure 1.

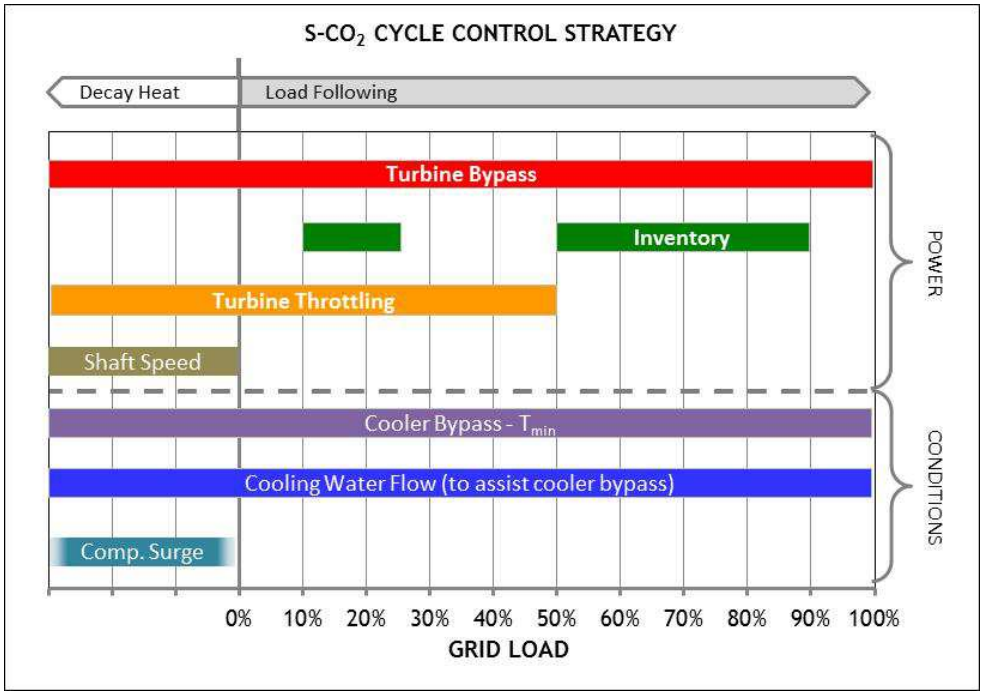

Figure 3. S-CO_2 Cycle Control Strategy.

The generator power control relies on a combination of turbine bypass, inventory control, and turbine throttling. As demonstrated in Figures 3 and 4(b), those control mechanisms are activated at different load levels to maximize the cycle efficiency at partial loads within the limits of the controls, such as inventory tank pressure and pressure rise across the throttling valve. Figure 3 also lists the cooler bypass control and the cooling water flow rate controls. Those controls were proven to be effective and necessary (Moisseytsev and Sienicki, 2008) for maintaining the compressor-inlet temperature close the design level during the load reduction transient, as demonstrated in Figure 4(k). More importantly, the combination of cooler bypass and water flow controls maintain the compressor-inlet temperature above the critical value during the entire transient, an important consideration in avoiding potentially damaging two-phase flow into the compressor, especially when the inlet pressure drops below the critical value as a result of inventory reduction in the cycle.

Figure 3 also includes compressor surge control. This control protects the compressor from surging by circulating the flow around each compressor when an approach to surge condition is detected. The compressor surge control is not used to control the generator power; it is implemented only to protect the compressors, if necessary. This control was not activated during the load following stage of the transient, but will be used to avoid compressor surge in the later stages of the transient.

As discussed above, the simulation in Figure 4 was carried out assuming autonomous reactor control. When the control action is applied to the S-CO_2 cycle, the heat removal by CO_2 in the sodium-to-CO_2 heat exchanger is reduced resulting in increasing sodium outlet temperature (Figure 4(m)). That higher temperature is eventually communicated to the core where it introduces, through the negative reactivity feedbacks (Figure 4(o)), negative reactivity which reduces the reactor power. The results show that the internal reactivity feedbacks are strong enough to match the heat removal in the RHX – the reactor power approaches the 40% of full power level (Figure 4(n)) by the end of the load reduction phase – without significant increase in reactor temperatures – the core-outlet temperature stays at or below the steady-state value, as shown in Figure 4(p). The hot-leg intermediate sodium temperatures rise slightly from 488 ℃ to about 500 ℃ during this stage.

Transition to Decay Heat Removal

The results discussed in the previous section demonstrate that the entire plant can effectively follow the electrical grid load over the entire range between 100% and 0% with the automatic control on the S-CO_2 side and autonomous operation on the reactor side. At the same time, the results in Figure 4 show that by the end of the load reduction stage the heat removal rate by the cycle is about 30% full power level. The reactor power, which follows the heat removal with some delay is about 40% full power at 1200 s. So, even though the plant does not produce any electrical power at this moment, the reactor still operates at 30-40% full power level. This is a result of decreasing cycle efficiency as the cycle conditions move further and further from the design point, eventually reaching zero efficiency at zero generator output.

If the reactor is to be disconnected from the grid after reaching zero electrical output and scrammed (i.e., shut down neutronically) (as it is usually the case), it would be unacceptable to have to operate the reactor at 30% power. The normal procedure would be to shut down the reactor in this case. Therefore, a control approach needs to be developed that facilitates the transition from 30% reactor power with zero net electrical output to decay heat levels (which initially contribute to about 6% power and reduce with time after shutdown). Note that it is not required any more to maintain net zero electrical output from the plant when the reactor is shut down; it is feasible to draw electrical power (if still available) from the grid to maintain reactor coolability for decay heat removal. However, if it can be shown that this operation can be completed for the S-CO_2 cycle with no external power demand, it would present significant safety benefits for reactor coolability by continuing to use the S-CO_2 cycle under, for example, loss-of-offsite power events.

To facilitate the reduction of reactor power after reaching zero plant output, an attempt was first made to use the same S-CO_2 cycle controls listed in Figure 3 beyond the ranges necessary for load following. The results of those calculations (Moisseytsev and Sienicki, 2011c) showed that the reactor power could indeed be reduced to approximately the 6% level. However, that cycle operation mode was so ineffective that in order to maintain the operation of the S-CO_2 compressors to keep CO_2 circulating in the cycle, a net power input of about 20% of the nominal plant capacity (i.e., about 80 MWe for a 400 MWe ABR-1000 plant) would be needed to ensure coolability of the reactor in the decay heat mode. Clearly, it would be too expensive to operate a plant in that regime and an alternative approach needed to be identified.

Alternatively, advantage can be taken of the fact that the transition to the decay heat removal mode in the transient analyzed here occurs after the net generator output to the grid reaches the zero level. As discussed above, at this point the generator can be safely disconnected from the grid. Once this happens, the grid-synchronous operation of turbomachinery is no longer a requirement even for the turbine and compressors located on the common shaft with the generator. Therefore, the shaft speed can now be changed more or less freely (subject to rotating inertia and blade load limitations).

To investigate the possibility of shaft speed control, it is assumed that the S-CO_2 turbomachinery shaft speed linearly decreases from 100 to 20% nominal following reduction of the grid load to zero. In this particular simulation, the user-specified shaft speed was assumed for simplicity. In reality, the shaft speed would be a controlled parameter, which would be maintained either by direct speed control mechanisms (such as load banks) or would naturally be established as a result of the power balance between the turbine, compressor, and generator, which could be operated in a motor regime supplying power to the shaft. In the case of zero net power output and in the absence of active direct shaft speed control, the shaft power balance and, therefore, its speed can be controlled by adjusting the power produced by the turbine, for example, by means of turbine bypass control. In the calculations shown below, the demanded net generator output is set to zero for the remainder of the transient. The automatic S-CO_2 cycle control still operates in the same regime as before; i.e., it adjusts the turbine power in order to match the given net generator output. So, with changing shaft speed and zero external demand, the automatic control strategy will calculate the necessary actions to maintain zero net output from the plant at a given speed. This, therefore, would be the same control action needed to match the specified shaft speed, if shaft power balance and automatic shaft speed control were to be implemented. However, simply to avoid possible additional uncertainty from automatic shaft speed control, in these calculations the shaft speed is assumed to be specified by user.

The shaft speed reduction rate of 10% per 80 seconds is arbitrarily assumed to be slow enough to avoid any rotating inertia limitations. The shaft speed reduction is assumed to continue linearly until the reactor

power level reaches decay heat levels. As will be shown in the results below, 20% of nominal shaft speed satisfies this criterion. As in the previous calculations, autonomous reactor operation is still assumed on the reactor side, meaning no active control of the reactor power or sodium pumps.

The results of the transient simulations are shown in Figure 4 between 1200 and 1840 seconds for the shaft speed reduction phase followed by operation for about 900 s without any external control to assess the stability of the system at those far-from-design conditions. As demonstrated in Figure 4, spinning down of the turbomachinery (Figure 4(e)) reduces the overall CO_2 flow rate in the cycle (Figure 4(g)) thus reducing the heat removal rate by the S-CO_2 cycle which reaches about 3% by the end of the transient simulation (Figure 4(d)). At this level, the reactor power is essentially equal to the decay heat power which is calculated to decrease to the same 3% level during the transient (Figure 4(n)). Therefore, the goals of the simulation, - reaching decay heat levels, - are shown to be achieved by the shaft speed control.

During the shaft speed reduction phase, the S-CO_2 cycle control mechanisms remain active to maintain the requested zero shaft power balance. The main control mechanism is turbine bypass control (Figure 4(b)). In addition, some limited action of turbine throttling is proven to be efficient in reducing the reactor power as a means to increase cycle efficiency (compared to turbine bypass control alone).

The results in Figure 4(k) also demonstrate that the compressor-inlet temperature starts to increase after 1200 seconds, i.e. simultaneously with the start of shaft speed reduction. Introduction of the shaft speed variation required the use of asynchronous, i.e. varying-speed, turbomachinery maps which requires extra storage for the shaft speed variable and, therefore, could not have the same resolution for other parameters, such as inlet temperature, as the synchronous maps. With reduced accuracy of the maps in the calculations, implementation of minimum temperature control results in numerical instability of the transient results. For these reasons, active minimum cycle temperature control was deactivated once the shaft speed started to decrease. However, as the results in Figure 4(k) show, in the absence of active control, the minimum temperature increases, meaning that operation in two-phase flow is not a concern in this regime. Besides, spinning down of the compressor results in an increase in the low cycle pressure such that it is shown to quickly return to levels above the critical value. Once the shaft speed reduction was completed and the compressor-inlet temperature was calculated to approach the critical point again later in the transient, minimum temperature control was restarted at about 2200 seconds and was shown once again to maintain the conditions above the critical temperature.

The results in Figure 4(i,j) also show that as the compressor speed starts to decrease, the operating range of the compressors, limited by surge on one side and choke on the other side, starts to decrease as well. At about 2100 seconds, the surge margin for the main compressor is calculated to approach the 10% flow value, which was selected as a triggering point for compressor surge control in Figure 3. At this point, flow recirculation around the main compressor was initiated in order to maintain the surge margin. As the results show, however, this recirculating flow was still not excessive such that increased compressor power requirements could still be satisfied by the turbine, without any need for external power supply. Some margin in turbine work still exists by the end of the transient simulation as shown by about a 10% open fraction in turbine bypass valve.

The same margin in turbine work can also be used to continue operation of the S-CO_2 cycle and the entire plant as the decay power continues to decrease with time. Eventually, though, a transition to another system designed for normal shutdown heat removal needs to be made. Such a system is necessary for maintenance and repair of the S-CO_2 cycle. The results of this study show that the normal shutdown heat removal system could be designed to remove no more than 3% power (or 6% for inclusion of emergency situations), which is much smaller than the 30% value from previous analysis partially reducing the SFR cost. The smaller heat removal requirement opens up the possibility of designing a passive system, for example, similar to the Direct Reactor Auxiliary Cooling System (DRACS) for emergency decay heat removal.

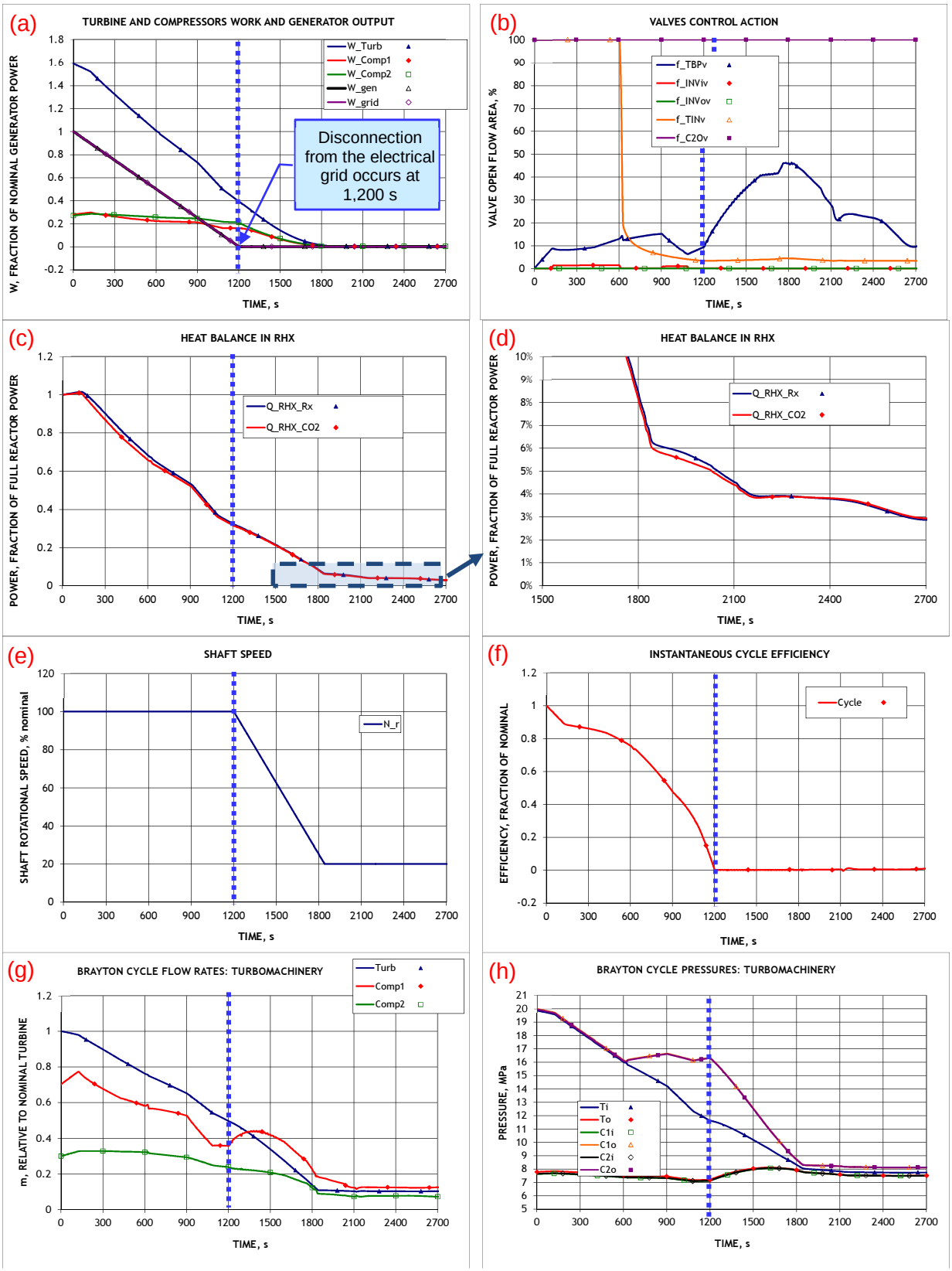

Figure 4. S-CO_2 Cycle Control Transient Results.

(continued on next page)

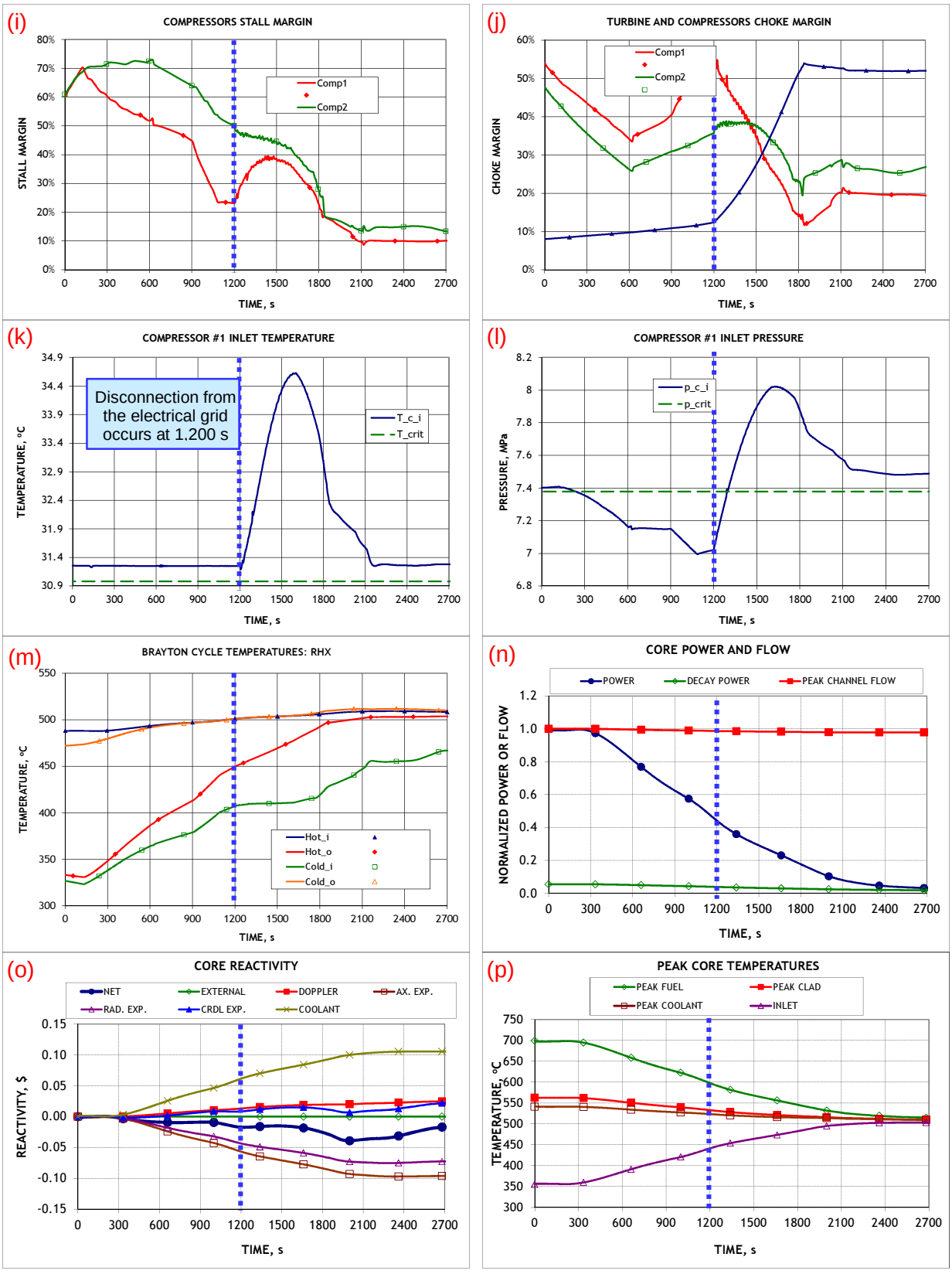

Figure 4. S-CO_2 Cycle Control Transient Results (Continued).

The results of the simulation show that the entire reactor can be brought from full power to decay heat removal levels in less than one hour. It is noted, however, that the simulated time was dictated by the assumed rates: first for the grid demand reduction at 5%/min; and then for the shaft speed reduction at 1% per 8 seconds. No attempt was made in this study to investigate how fast the reactor can be brought from full power to decay heat levels. Still, based on the favorable response of the entire system and the fact that none of the limiting factors are approached in transient, it is believed that the transiting can be carried out at a faster rate, at least from a thermal hydraulic perspective. At those rates, other considerations, such as thermal stresses in the structural materials, will become more important.

S-CO_2 CYCLE CONTROL WITH ACTIVE REACTOR CONTROL

In the previous analysis described above, it has been demonstrated that the cycle coupled to the 1000 MWt ABR-1000 SFR design can effectively follow the electrical grid demand by means of automatic cycle control, even with autonomous reactor operation, where no active control (e.g., motion of control rods or changing of primary or intermediate sodium pump speeds) is applied on the reactor side such that the reactor responds to the changing conditions solely by means of the internal reactivity feedbacks. Autonomous reactor operation has obvious safety advantages through elimination of failure modes related to active control, and would be desirable for SFR Small Modular Reactors (SMRs) in enabling autonomous load following and reducing operator workload. However, its nature implies that due to the overall negative reactivity feedback with increasing temperature, the reactor power can only be reduced in response to rising reactor temperatures, at least at some locations. The results of the previous analysis indeed demonstrated that even though the hot-side (e.g., core-outlet) temperatures remain at about the same level during the load reduction transient (as a result of the strong negative reactivity feedbacks of the ABR-1000 fast spectrum core with metallic fuel and sodium coolant), the cold-leg temperatures on both the primary and intermediate sodium sides do increase at lower loads. This temperature increase may complicate the structural design or, alternatively, may increase the reactor cost by a requirement that the cold-leg structures (e.g., the reactor vessel) and piping are to be designed for temperatures higher than full-power values.

In order to preclude temperature increases in the cold legs of the reactor loops, active reactor controls are usually implemented. To see how this effective reactor control affects the S-CO_2 cycle behavior, a plant control mode involving active control on both the reactor and S-CO_2 side was simulated with the coupled PDC-SAS4A/SASSYS-1 codes. The intermediate sodium temperature at the RHX outlet is set to be maintained by means of the flow rate (i.e., pump) control. When the heat demand to the reactor from the cycle decreases, the sodium pumps slow down reducing the intermediate sodium flow rate and maintaining the sodium temperatures. At the same time, reducing the intermediate sodium flow rate leads to reduced heat removal in the Intermediate Heat Exchanger (IHX) leading to hotter primary sodium at the IHX outlet. Therefore, similar flow rate control is implemented on the primary sodium side in order to maintain the IHX-outlet and, therefore, core inlet temperatures. Similarly, reduced primary coolant flow rate through the core results in an increased core outlet temperature which, in turn, is controlled by adjusting the reactor power by means of the control rods. In the case of idealized controls, the primary and intermediate sodium temperatures would be maintained at the design level almost everywhere and the reactor power would match the S-CO_2 cycle demand for any variation of the cycle conditions.

Although the SAS4A/SASSYS-1 code has its own reactor control module it has some limitations which complicate its use in coupled PDC-SAS4A/SASSYS-1 calculations. Instead, an approach to calculate the reactor control action by the PDC was implemented. The required control actions, i.e. sodium pump torques and the core external reactivity, is provided to SAS4A/SASSYS-1 in the form of time-dependent tables, similar to the tables already used in the existing PDC-SAS4A/SASSYS-1 coupling scheme to calculate the intermediate sodium temperature change in the RHX by the PDC and provide the results to SAS4A/SASSYS-1 on each time step.

Results with Fixed Sodium Temperatures

To investigate the effects of the developed reactor active controls on the transient nuclear power plant response, a linear grid load reduction transient at 5%/min rate from 100% to 60% (in 480 s) followed by operation at the 60% level was first simulated with both enabled and disabled reactor controls. The results, as expected, demonstrate the benefits of active reactor control with the calculation of less varying

reactor temperatures, including the RHX-outlet, IHX-outlet, and the core-inlet temperatures, and a much better balance between power and flows on the reactor side throughout the transient.

Those results, though, were obtained for a partial 40% load reduction. An attempt to carry out further load reduction showed that there is a limit on the selected reactor control. Figure 5 shows the behavior of the RHX cold-end temperatures (inlet on the CO_2 side and outlet on the sodium side) for a linear load reduction all the way to 0%. An oscillating and unstable behavior is clearly seen in this figure. The instabilities are caused by the behavior of the CO_2 temperature at the RHX inlet at reduced grid loads. When inventory control starts to act on the S-CO_2 cycle side (after 120 s), the CO_2 flow rate in the system is reduced leading to more efficient operation of the High Temperature Recuperator (HTR) and, therefore, to a gradual increase in the CO_2 temperature at the HTR outlet or RHX inlet. By about 500 s, the CO_2 temperature increases to the steady-state value of the sodium temperature at the RHX outlet. At this point, no action on the intermediate sodium pump can bring the sodium temperature below that of CO_2 inlet, as required by the current setup of the control system where the target sodium temperature is the same throughout the transient.

Several options were investigated to avoid the undesirable system behavior observed in Figure 5. Each of the considered options is discussed below in details.

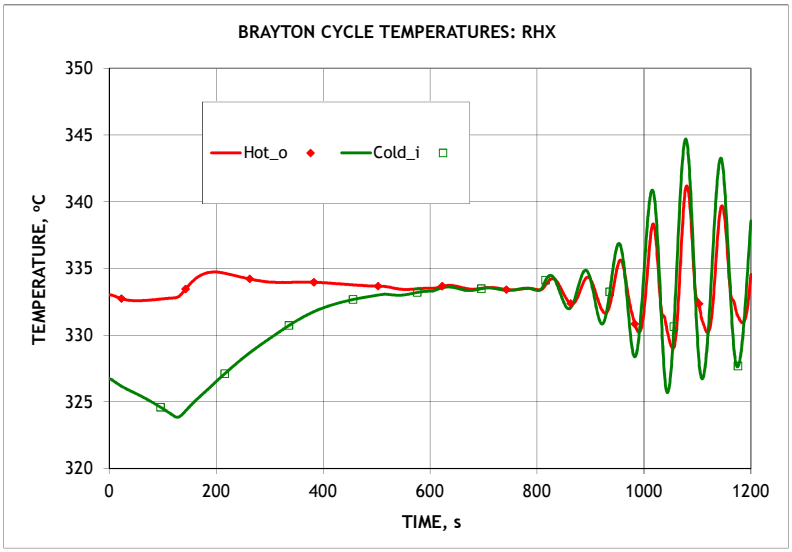

Figure 5. Temperatures on the Cold End of the HTR.

Margin to CO_2 RHX Inlet Temperature

One solution to this problem would be to change the target sodium RHX outlet temperature to maintain some margin (for example, 5 ℃) above the CO_2 RHX-inlet temperature. Calculations with this limitation indeed improved the stability of the system. However, this limit also almost eliminates the benefits of active reactor control, since it allows the cold-side sodium temperatures to increase, much like in the autonomous control case.

Reduced Inventory Control Action

A possibility to maintain the RHX inlet temperature was realized from analysis of the results in Figure 5. The RHX inlet temperature on the S-CO_2 cycle side starts to increase after 120 s, i.e., at 90 % load when inventory control is initiated. Before that time, when only turbine bypass control is active, the RHX inlet temperature even decreases. With turbine bypass control, the CO_2 flow rate in the lower portion of the cycle (in the compressors and recuperators) is increasing such that the CO_2 heatup in the HTR is reduced. Since the CO_2 temperature at the RHX inlet reduces with the turbine bypass action and increases with the inventory control, an analysis was carried out to determine the combination of these two controls which results in a constant CO_2 temperature at the RHX inlet. The results show that the

temperatures at the cold end of the RHX can be maintained, if the inventory control is set up to remove 40% of the CO_2 mass, compared to the normal control set up.

However, since inventory control provides the most efficient operation at reduced loads, reducing its action leads to lower cycle efficiency. Because of this inefficiency in the cycle operation at reduced loads, it is concluded that maintaining the CO_2 temperature at the RHX inlet by means of inventory control variation is not a preferred choice and other options should be investigated.

Implementation of Recuperator Bypass for RHX-Inlet Temperature Control

Since the range of the active reactor-side controls was found to be limited by the CO_2 temperature at the RHX inlet, the CO_2 temperature at the RHX inlet can be actively controlled by means of HTR bypass. When the RHX inlet temperature increases too much, the cycle layout may be designed such that a portion of the CO_2 flow bypasses the HTR, thus reducing the CO_2 heating in the recuperator. To investigate the effect of such a control action on the cycle performance, HTR bypass control was implemented in the PDC.

With active HTR bypass, the results earlier in the transient are the same as those in Figure 5. At about 170 s, the RHX inlet temperature reaches the steady-state value of 326 ℃ and the recuperator bypass control is initiated. As the flow rate in the system continues to decrease with continuing inventory removal, more of the HTR bypass is needed to maintain the RHX inlet temperature.

In addition to maintaining the RHX CO_2 inlet temperature, the recuperator bypass action has another effect on the system behavior. As less flow goes through the HTR on the cold side, less heat is removed from the hot side flow, leading to increasing temperature at the HTR hot side outlet. Consequently, the temperature entering the low temperature recuperator (LTR) on the hot side starts to increase as well. As a result, the temperatures on the LTR cold outlet, and therefore, the HTR cold inlet, continue to increase during the transient. By 900 s, temperatures close to 390 ℃ are calculated at the LTR hot end, resulting in about 330 ℃ at the HTR cold side inlet (after mixing with the flow from the recompressing compressor). With 330 ℃ at the HTR inlet, it is no longer possible to maintain 326 ℃ at the HTR outlet (or RHX inlet), no matter what the bypass fraction is. Consequently, the HTR bypass flow fraction is calculated to be 100% by this time and the calculations are terminated shortly before 900 s at conditions of zero flow though the HTR.

Reduction in Core Outlet Temperature

The results obtained so far have shown that the decreasing temperature change in the turbine and across the RHX is a natural result of the cycle behavior under reduced load and reduced flow conditions. If the core outlet temperature is maintained in a transient, either by active reactor control or (autonomously) purely through the reactivity feedbacks, the cold side temperatures would naturally increase, unless an undesirable control scheme is used to maintain the cold side temperatures. Alternatively, if one wants to fix the cold side temperatures in load reduction transients, then the hot side temperatures, including the core outlet temperature, need to be reduced with grid load. Of course, a disadvantage of this approach is the lower CO_2 turbine inlet temperature which is expected to reduce the cycle efficiency. The results of the autonomous reactor mode calculations (presented above) showed that if no temperature control is implemented on the reactor side, then the CO_2 temperature at the RHX inlet would increase by 105 ℃ when the grid load is reduced from 100% to 0%. Those results also showed that this increase is almost linear and occurs when cycle controls other than turbine bypass are activated, i.e., for loads below 90%. Therefore, in an attempt to maintain the CO_2 RHX inlet temperature, the reactor side power control was configured to linearly decrease the core outlet temperature by 105 ℃ (from 510 ℃ to 405 ℃) between 90% and 0% loads. It is expected, however, that due to the thermal inertia of the reactor side coolant volumes and structures, any change in the core outlet temperature will be communicated to the S-CO_2 cycle with a significant delay. Based on the coolant masses, it is estimated that the change in the core outlet temperature will affect the CO_2 temperatures with a delay of about 500-1000 seconds. During this period, the CO_2 temperature at the RHX inlet will continue to rise, unless active temperature control, e.g., recuperator bypass, is implemented.

Some results of the load reduction transient simulation with decreasing core outlet temperature are shown in Figure 6. In this simulation, the recuperator bypass control is not activated such that the CO_2

RHX inlet temperature is allowed to rise. The results show that the intermediate sodium temperature at the RHX outlet increases from 333 ℃ at steady-stat e to 355 ℃ at the peak at 1100 s. The variation of the primary sodium temperature at the IHX inlet is limited to about 3 ℃. A similar variation of less than 3 ℃ is calculated for the core inlet temperature.

The simulation in Figure 6 was extended to include an additional 1000 s after the load reduction is complete at 1200 s. The results in Figure 6 demonstrate that about this much time is needed to stabilize all of the temperatures following the completion of the core outlet temperature adjustment at 1200 s. By the end of the transient at 2200 s, the temperatures at the cold end of the RHX basically return to the full power level. The CO_2 temperature at the RHX inlet stabilizes at 327.2 °C, compared to 326.7 ℃ at full power. This result confirms that selection of a 105 ℃ reduction in the core outlet temperature is appropriate. Both the reactor power and the heat removal rate by CO_2 at the RHX reach about the 28% level by the end of the transient.

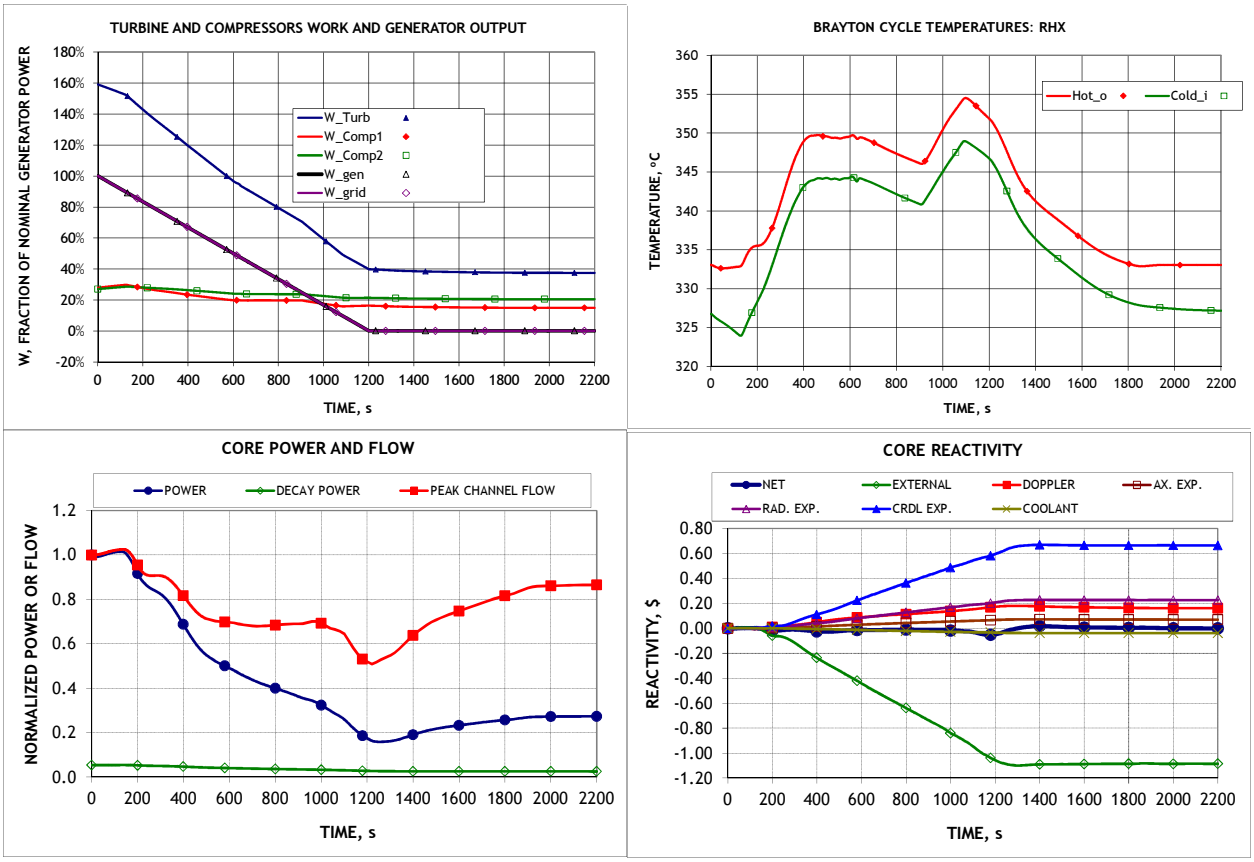

Figure 6. Load Reduction Results with Decreasing Core-Outlet Temperature.

ANL PLANT DYNAMICS CODE VALIDATION

The analysis described above was carried out using the Plant Dynamics Code being developed at ANL specifically for the S-CO_2 cycle. In parallel to the code development, an effort is being devoted to verify and validate the code. From the code validation purposes, the immaturity of the S-CO_2 cycle concept presents some challenges. Until recently, virtually no experimental data on S-CO_2 cycle components and integral cycle performance were available. For these reasons, verification of the PDC in its early development was mostly limited to benchmark calculations against similar codes being developed for S-CO_2 cycle analysis (Vilim and Moisseytsev, 2008).

Later, limited validation of the PDC models on an individual component basis was carried out using available experimental data obtained from facilities directed at demonstrating the performance of individual components. Specific component tests were selected for comparison to address significant

features of the S-CO_2 cycle, such as the effect of properties variation near the critical point. For example, experimental work focused on the heat exchangers, especially the cooler and the low temperature recuperator since they operate very close to the critical point, and the CO_2 compressors designed to operate in the proximity of the critical point (Lomperski et.al, 2006; Moisseytsev et.al, 2010; Moisseytsev and Sienicki, 2011d).

Later (Moisseytsev and Sienicki, 2012), the steady-state part of the PDC was validated against the experimental data obtained at the S-CO_2 loop operated by Sandia National Laboratories (SNL). That SNL S-CO_2 loop was constructed for SNL at Barber-Nichols, Inc. (BNI) in a staged fashion with the ultimate goal of demonstrating a complete recompression S-CO_2 cycle and all of its principal components, including two compressors, turbines, two recuperators, a water cooler, and heat source heat exchangers simulated by electrical heater units. For that work, one of the earlier configurations featuring a single turbine-alternator-compressor (TAC) unit and a single recuperator was analyzed. During the simulation of the SNL S-CO_2 loop with the PDC, several challenges in modeling the loop were identified. For example, a noticeable heat loss in the turbine volute was discovered which could not be accurately measured in the experiments. Therefore, some assumptions had to be made in the PDC modeling to account for this and other uncertainties in the experimental setup. However, despite all the uncertainties and assumptions, reasonably good agreement was achieved between the code predictions and the measured data for steady-state conditions.

The next logical step in the PDC code validation would be comparing the code predictions with experimental data in transient conditions. However, the particular configuration used for the previous steady-state analysis was not suitable, since the majority of the transient run involved subcritical conditions at the compressor inlet. The PDC was not developed to analyze subcritical conditions which are not representative of commercial S-CO_2 cycles. Fortunately, other transient data was identified and made available to ANL from the July 2011 experimental runs.

The SNL S-CO_2 Loop experiment data from July 14, 2011 was selected for further simulation with the Plant Dynamics Code. For the majority of this experimental run, the conditions at the compressor inlet were maintained above the critical point. The loop layout for this run and the measured experimental data are presented in (Conboy et.al, 2012). The loop layout is also shown schematically on the top plot of Figure 7 in this paper. Compared to the previous work, the main difference in the cycle layout is the addition of the high-temperature recuperator.

Since the PDC calculations start from steady-state conditions, a point in the run had to be selected where the loop state can be modeled with steady-state equations. A data point at 3356 seconds was selected as a starting point for the transient calculations with the PDC, since it represents the best combination of preceding continuous operation for some time without either rotational speed (RPM) or heater control changes as well as supercritical conditions at the compressor inlet. Since the PDC calculations start with time zero, the “PDC time” referred to in this paper is 3356 s less the recorded experimental time. Unless clearly specified otherwise, all further plots in this paper will be presented on the PDC time scale.

Several assumptions and model modifications had to be made for the modeling of the SNL S-CO_2 Loop:

- Little information on the internal configuration of the HTR was provided to ANL. Therefore, several assumptions on the HTR configuration (e.g., zigzag channel angle) had to be made in order to develop a model for the PDC. To account for the less than perfect steady-state conditions at 3356 s and for the heat losses in the HTR, it was decided to include a heat loss into the pipe connecting the HTR cold side outlet with the heater. The magnitude of the heat loss was selected to obtain good agreement on the heater-inlet temperature given the performance prediction of the HTR.
- Due to numerical issues resolving too close temperatures in the LTR and since the LTR is not significantly changing the fluid temperatures in this particular run, it was decided to exclude this heat exchanger from the PDC modeling of the loop. The effects of the LTR on the pressure drop and the thermal inertia of the system would need to be evaluated based on the transient results. If needed, though, these factors could be included into the HTR model.
- An initial attempt to apply the as-measured inlet conditions in Figure 7 to the compressor model resulted in significant under prediction of the outlet temperature with simultaneous over prediction

of the outlet pressure. A subsequent analysis revealed that with the direct input of the inlet pressure and temperature there is a significant over prediction on the compressor-inlet density which was also measured in the experiments. The inlet density is considered to be a better indication of the CO_2 properties at the compressor inlet since the properties near the critical point are much less sensitive to the uncertainty in density than to that in pressure and temperature. When the inlet pressure and temperature were adjusted (within the measurement uncertainty) to match the measured inlet density, a much better agreement was obtained on both outlet pressure and temperature. Consequently, the compressor-inlet conditions with matching inlet density were adopted for the steady-state conditions for the PDC model.

The comparison of the steady-state PDC prediction with the experimental data is shown in Figure 7. The top plot in Figure 7 shows the instantaneous readings at the 3356 s point of the experimental time. The bottom plot in Figure 7 demonstrates the results obtained with the steady-state part of the PDC.

The compressor-inlet conditions (pressure and temperature) were intentionally modified to match the measured compressor-inlet density, as described above. With this modification, the compressor-outlet conditions are predicted very accurately. Also as discussed above, the LTR is not currently included into the PDC model, so it has no effect on the calculated temperatures and pressures (the LTR is shown in Figure 7 only for comparison with the experimental configuration).

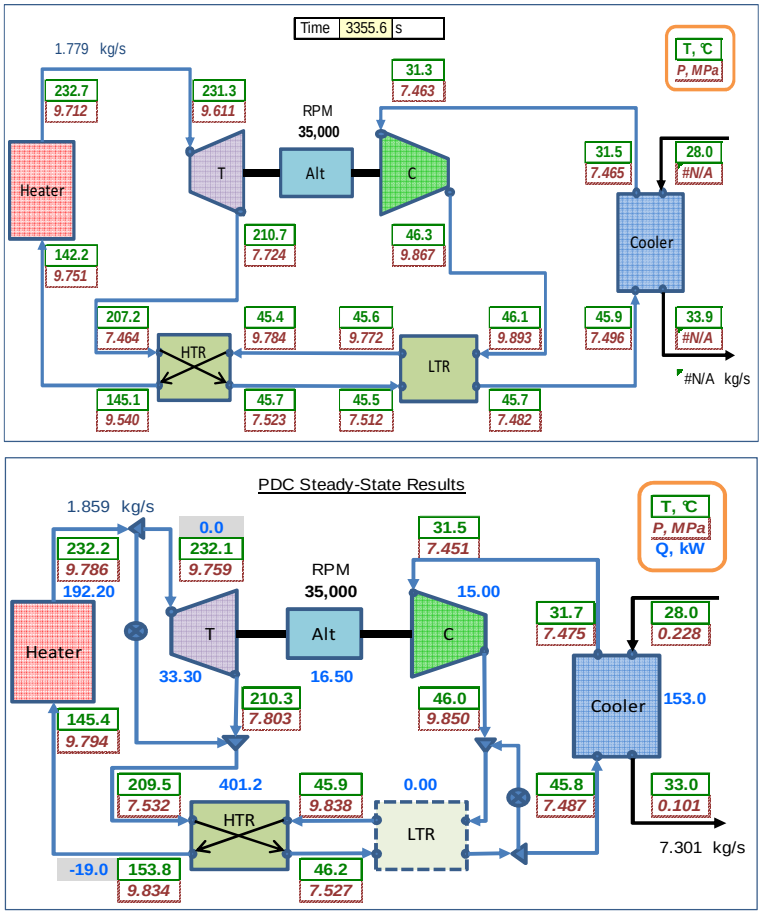

Figure 7. SNL S-CO_2 Loop Layout for July 2011 Run -Experimental Conditions (Top) and Steady-State PDC Results (Bottom).

To compensate for the heat imbalance in the HTR, a heat loss was added to the pipe connecting the HTR with the heater. Using the PDC steady-state model, it was determined that a significant heat loss adjustment of 19 kW was needed in order to match the heater-inlet temperature and, therefore, the calculated CO_2 flow rate in the heater and elsewhere, and to achieve the temperature and pressure

balance in the entire system. With this significant heat loss, it was not necessary to include an additional loss in the turbine volute (or in the turbine inlet pipe), as in the previous simulation. Thus, the heat loss in the HTR-heater pipe represents the heat loss in the entire system. This does not mean that the heat losses in the turbine volute or elsewhere in the loop are not significant. The heat loss is simply applied at one place for simplicity of the calculations; a more detailed distribution of the heat loss throughout the system would be more prototypical of the actual conditions. However, modeling that would require more detailed knowledge on the system behavior at various steady-state and transient conditions; i.e., more experimental data for this particular loop configuration would be needed.

Even with the significant heat loss in the pipe upstream of the heater, the heater-inlet temperature is still about 3 ℃ higher in the model than the measured va lue. This difference resulted in prediction of a slightly higher (by 4.5%) flow rate in the system in order to match the heater-outlet conditions. The turbine-outlet conditions are matched accurately by the code. To simulate the apparent significant pressure drop in the turbine-HTR pipe, an artificial valve was added to this pipe in the PDC model.

The conditions at the HTR hot side outlet, around the cooler, and back to compressor inlet are all matched closely by the code, within the experimental uncertainty.

The TAC drain flow path driven by the Hydropac pump implemented in the SNL S-CO_2 Loop is not included into the PDC model. This flow rate is at least an order of magnitude less than the main loop flow rate.

Overall, the results in Figure 7 were judged satisfactory, given the fundamental differences arising from simulating experiment conditions that have not achieved a true steady state with the steady-state equations. Therefore, the calculations of the transient part could proceed from this point.

Dynamic Simulation of SNL S-CO_2 Loop with the PDC

In order to be able to simulate transient behavior of the loop with the PDC, several modifications were introduced to the code. These modifications were limited to simulating the particular controls implemented in the SNL S-CO_2 loop such as the electrical heater control and the control of the cooling water flow rate by means of a bypass valve. Only for the heaters, which are currently represented using the existing PDC shell-and-tube heat exchanger model, some modifications to the code equations were introduced in order to simulate the direct heat input into the heat exchanger “tubes”.

Starting from the steady-state conditions shown in Figure 7, the transient simulation of the July 2011 experiment with the PDC was carried out. The transient was defined by the external input simulating the SNL Loop control by the operators. That external input is described below.

External Input

As discussed above, the SNL S-CO_2 Loop experiments are defined by the operator input for the TAC rotational speed, heater power, and water flow rate controls. For the heater control, the automatic heater control was simulated for the July 2011 experiment. The heater-outlet set temperature was directly imported from the recorded target temperature in the experiment. No other input for the heater was needed, except for the flags which define the automatic control option.

Similar to the heater control, an automatic water flow control was used in this simulation with the option of controlling the cooler-outlet temperature. The as-recorded cooler-outlet temperature was used as an input for the target temperature for the water flow control. All other parameters of the water control, including the PID coefficients, were retained from those developed for analysis of the full-size systems; no attempts to optimize the control for this particular application were made.

The cooler inlet water temperature was supplied to the PDC from the as-measured data without any modifications.

The TAC speed input was adopted from “Target RPM” input which is also recorded in the experimental data. A 5 second delay at each RPM change was introduced to better simulate the actual TAC speed.

These external controls were the only inputs to the PDC to define the transient. No other inputs were needed. (For example, the system pressures are calculated in a transient by the PDC, rather than being

supplied as external input, based on calculated CO_2 mass redistribution.) Also, all other controls, previously incorporated into the PDC, were disabled for this simulation. The simulation was carried out for 2500 seconds PDC time which is equivalent to the time interval from 3356 s through 5856 s of the recorded experimental time.

The turbomachinery maps were re-calculated for this particular transient to cover the range of operating parameters recorded in the test.

Transient Results

The detailed discussion of results of the PDC transient simulation is provided in (Moisseytsev and Sienicki, 2013). Some of the results are presented in Figure 8 in comparison with the as-recorded data. In this figure, the PDC results are shown in thinner lines and are denoted with a symbol while the experimental data is shown with thicker lines without symbols. The first few plots in Figure 8 show the comparison between the calculated and measured temperatures around the loop.

Despite all of the special assumptions, the transient results obtained with the PDC are close to the actual experimental data. Almost all temperatures showed good agreement with the experimental readings. The noticeable exception was the heater inlet temperature which is consistently underpredicted by the code. The analysis has shown that this is the result of incorporating the heat loss into the HTR-heater pipe. By comparing the PDC results with the experimental data later in the transient, it was discovered that this heat loss wasn't as large as was needed for the steady-state simulation. So, the discrepancy in the heater-inlet temperature prediction is believed to be a result of the adjustment needed to simulate an imperfectly balanced system with the steady-state equations.

The other findings from the temperature comparison suggest that the thermal inertia of the HTR may be underestimated by the code. This may be an effect of not knowing the exact internal configuration of the HTR. It may also be a consequence of not including the LTR mass into the PDC model.

The results also show that the effect of the heat transfer between the CO_2 and the pipe walls not currently modeled in the PDC has a somewhat noticeable effect on the temperatures during the rapid temperature changes, especially at the turbine inlet. This effect, though, is expected to be smaller (in relative terms) for larger systems with larger piping diameters.

Comparing the pressure and density predictions, it was observed that the pressures on the low side of the cycle were predicted very accurately by the code. On the high side, there is a difference between the code predictions and the actual data, indicating that the turbine and compressor performances may be overestimated by the code, especially at higher RPM.

Based on the results obtained, the ongoing work on the PDC validation with the SNL data is focused on the following directions:

- Better simulation of the heat losses in the system possibly with a distributed loss model. It is noted though that more experiments specifically designed to characterize the heat loss parameters at various conditions would be needed to accurately simulate the distributed heat loss in the loop.
- Finding experiment data more suitable for the steady-state simulation for the starting point of transient simulation.
- Refining the HTR model, if more design data is made available to ANL.
- Carrying out more comparisons of the turbine and compressor performance predictions with the experimental data, especially at higher rotational speeds.
- Including the effect of the LTR on the pressure drops and the thermal inertia.
- Modeling the heat transfer and heat losses in the pipes.
- Continue to apply the PDC to other experiment runs including different loop configurations to investigate whether the effects identified in this report are specific to the particular configuration and conditions simulated in this study.

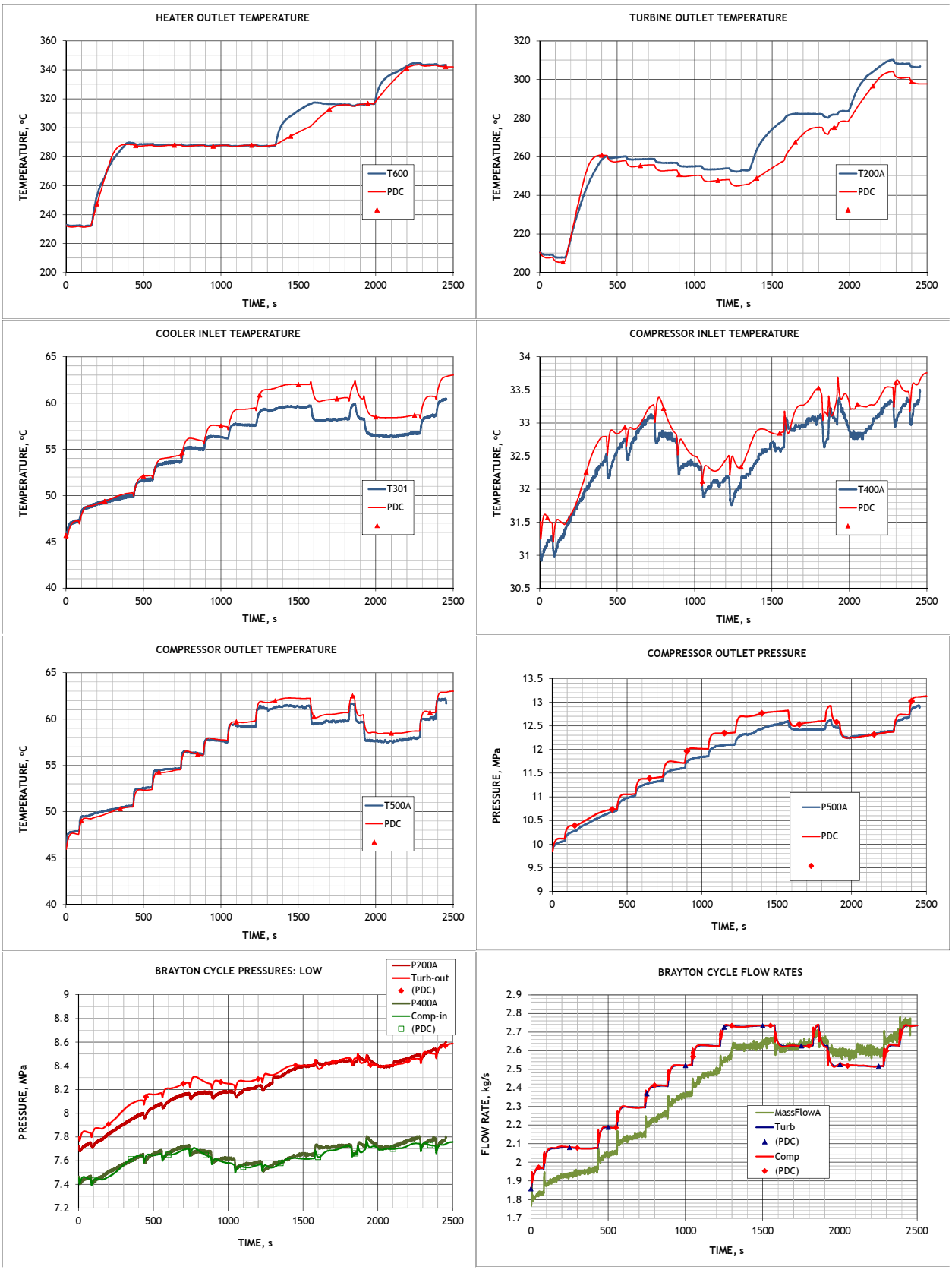

Figure 8. PDC Transient Results for SNL Loop.

SUMMARY AND CONCLUSIONS

The paper desicribes the progress achieved in S-CO_2 cycle analysis at ANL since 2011 S-CO_2 Power Cycle Symposium. The improvement and use of the ANL Plant Dynamics Code for the S-CO_2 cycle control investigation has been continued.

A new approach was developed to couple the Plant Dynamics Code for S-CO_2 cycle calculations with SAS4A/SASSYS-1 calculations for the SFR reactor side. The coupling was done using an executable file for the SAS4A/SASSYS-1 code, avoiding the need for modification of the SAS4A/SASSYS-1 source code. The new code system allows use of the full capabilities of both codes such that whole-plant transients can now be simulated without additional user interaction.

A control strategy for the supercritical carbon dioxide (S-CO_2) Brayton cycle has been developed enabling cycle operation in load following from 100% power all the way to zero grid demand as well as removal of power from an autonomous load following SFR down to decay heat levels such that the S-CO_2 cycle can be used to cool the reactor until switchover to the normal shutdown heat removal system or a passive decay heat removal system. To investigate the effectiveness of cycle controls, calculations were carried out using the coupled PDC-SAS4A/SASSYS-1 code for a linear load reduction transient for a 1000 MWt metallic-fueled SFR with autonomous load following. The results for the load following stage of the transient show a favorable response of the entire plant to the load reduction event. The S-CO_2 cycle control system is able to follow the load over its entire range – from 100% to 0%. Use of a combination of various control mechanisms allows maximizing cycle efficiency at various loads

The capability to operate the cycle at initial decay heat levels has been demonstrated. It has been found that this capability can be achieved by introducing a new control mechanism involving shaft speed control for the common shaft joining the turbine and two compressors following reduction of the load demand from the electrical grid to zero. Following disconnection of the generator from the electrical grid, heat is removed from the intermediate sodium circuit through the sodium-to-CO_2 heat exchanger, the turbine solely drives the two compressors, and heat is rejected from the cycle through the CO_2-to-water cooler. No deliberate motion of control rods or adjustment of sodium pump speeds is assumed to take place. It is assumed that the S-CO_2 turbomachinery shaft speed linearly decreases from 100 to 20% nominal following reduction of the grid load to zero. The reactor power is calculated to autonomously decrease down to 3% nominal providing a lengthy window in time for switchover to the normal shutdown heat removal system or for passive emergency decay heat removal to become effective.

Implementation of active reactor control involving motion of control rods to reduce the core outlet temperature and changing of the primary and intermediate sodium pump speeds to seek to maintain the sodium cold leg temperatures has been found to provide significant benefits over purely autonomous reactor behavior for specific load following transients. Overall, decreasing the core outlet temperature through active control provides the most favorable results in terms of both temperatures and nuclear power plant efficiency. Decreasing the core outlet temperature eliminates the effects of significant thermal transients involving temperature increases (and subsequent decreases) in the sodium cold legs but introduces thermal transients for structures exposed to higher temperature sodium. The results suggest that the efficiency decrease from the lower turbine inlet temperature accompanying decrease of the core outlet temperature does not affect the cycle performance significantly at reduced loads. If small temperature increases in the sodium cold legs can be tolerated, then no recuperator bypass action is needed and the cycle operate very closely to the optimal regime. The new control mechanism of recuperator bypass on the S-CO_2 cycle side has been introduced to maintain the cold side temperatures.

The PDC validation effort is currently focusing on simulation of the experimental data obtained at the SNL small-scale S-CO_2 integral test facility. In order to be able to simulate transient behavior of the loop with the PDC, several modifications were introduced to the code. These modifications were limited to simulating the particular controls implemented in the SNL S-CO_2 loop such as the electrical heater control and the control of the cooling water flow rate by means of a bypass valve. Only for the heaters, which are currently represented using the existing PDC shell-and-tube heat exchanger model, some modifications to the code equations were introduced in order to simulate the direct heat input into the heat exchanger “tubes”. Some assumptions had to be made for the transient simulation of the July 2011 configuration of the SNL S-CO_2 loop, such as excluding the low temperature recuperator from the PDC model, simulating all of the heat losses in the system to occur in the HTR-heater pipe, and using an automatic water flow

rate control in transients in order to match the recorded temperature at the cooler outlet. Despite all of these assumptions, the transient results obtained with the PDC are close to the actual experimental data. Almost all temperatures show good agreement with the experimental readings. The noticeable exception was the heater inlet temperature which is consistently underpredicted by the code. The analysis has shown that this is the result of incorporating the heat loss into the HTR-heater pipe. By comparing the PDC results with the experimental data later in the transient, it was discovered that this heat loss wasn't as large as was needed for the steady-state simulation. So, the discrepancy in the heater-inlet temperature prediction is believed to be a result of the adjustment needed to simulate an imperfectly balanced system with the steady-state equations. Comparing the pressure and density predictions, it is observed that the pressures on the low side of the cycle are predicted very accurately by the code. On the high side, there is a difference between the code predictions and the actual data, indicating that the turbine and compressor performances may be overestimated by the code, especially at higher RPM.

REFERENCES

Cahalan, J. E., Tentner, A. M., and Morris, E. E., 1994, "Advanced LMR Safety Analysis Capabilities in the SASSYS-1 and SAS4A Computer Codes," Proc. of the International Topical Meeting on Advanced Reactor Safety, 1994, Vol. 2, p. 1038, American Nuclear Society, Pittsburgh, April 17-21.

Conboy, T., Wright, S., Pasch, J., Fleming, D., Rochau, G., and Fuller, R., 2012, "Performance Characteristics of an Operating Supercritical CO_2 Brayton Cycle," GT2012-68415, Proceedings of the ASME Turbo Expo 2012, June 11-15, Copenhagen, Denmark.

Lomperski, S. Cho, D. Song, H. and Tokuhiro, A., 2006, "Testing of a Compact Heat Exchanger for Use as the Cooler in a Supercritical CO_2 Brayton Cycle," Paper 6075, Proceedings of 2006 International Congress on Advances in Nuclear Power Plants (ICAPP 06), Reno, NV, June 4-8.

Moisseytsev, A. and Sienicki, J. J., 2006, "Automatic Control Strategy Development for the Supercritical CO_2 Brayton Cycle for LFR Autonomous Load Following," Paper 6074, Proceedings of 2006 International Congress on Advances in Nuclear Power Plants, ICAPP'06, Reno, NV, June 4-8.

Moisseytsev, A., 2007, "Development of a Plant Dynamics Computer Code for Analysis of a Supercritical CO_2 Cycle Energy Converter," presentation at Supercritical CO_2 Power Cycle for Next Generation Systems Symposium, MIT, March 6.

Moisseytsev, A. and Sienicki, J. J., 2006, "Development of a Plant Dynamics Computer Code for Analysis of a Supercritical Carbon Dioxide Brayton Cycle Energy Converter Coupled to a Natural Circulation Lead-Cooled Fast Reactor," ANL-06/27, Argonne National Laboratory.

Moisseytsev, A. and Sienicki, J. J., 2008, "Controllability of the Supercritical Carbon Dioxide Brayton Cycle Near the Critical Point," Paper 8203, 2008 International Congress on Advances in Nuclear Power Plants (ICAPP 2008), Anaheim, CA, June 8-13.

Moisseytsev, A. and Sienicki, J. J., 2009, "ANL Plant Dynamics Code and Control Strategy Development for the Supercritical Carbon Dioxide Brayton Cycle," presented at $SCCO_2$ Power Cycle Symposium 2009, RPI, Troy, NY, April 29-30.

Moisseytsev, A. and Sienicki, J. J., 2010, "Investigation of Plant Control Strategies for the Supercritical CO_2 Brayton Cycle for a Sodium-Cooled Fast Reactor using the Plant Dynamics Code," ANL-GenIV-147, Argonne National Laboratory, September 9.

Moisseytsev, A. and Sienicki, J. J., Cho, D. H., and Thomas, M. R., 2010, "Comparison of Heat Exchanger Modeling with Data from CO_2-to-CO_2 Printed Circuit Heat Exchanger Performance Tests," Paper 10123, 2010 International Congress on Advances in Nuclear Power Plants (ICAPP 10), San Diego, CA, June 13-17.

Moisseytsev, A. and Sienicki, J. J., 2011a, "Investigation of Plant Control Strategies for a Supercritical CO_2 Brayton Cycle Coupled to a Sodium-Cooled Fast Reactor using the ANL Plant Dynamics Code," 2011 Supercritical CO_2 Power Cycle Symposium, Boulder, CO, May 24-25.

Moisseytsev, A. and Sienicki, J. J., 2011b, “Autonomous Load Following Behavior of a Sodium-Cooled Fast Reactor with a Supercritical Carbon Dioxide Brayton Cycle,” Paper 11192, 2011 International Congress on Advances in Nuclear Power Plants (ICAPP 11), Nice, France, May 2-5.

Moisseytsev, A. and Sienicki, J. J., 2011c, “Development of the ANL Plant Dynamics Code and Control Strategies for the Supercritical Carbon Dioxide Brayton Cycle and Code Validation with Data from the Sandia Small-Scale Supercritical Carbon Dioxide Brayton Cycle Test Loop,” ANL-ARC-218, Argonne National Laboratory, September 29.

Moisseytsev, A. and Sienicki, J. J., 2011d, “Validation of the ANL Plant Dynamics Code Compressor Model with SNL/BNI Compressor Test Data,” 2011 Supercritical CO_2 Power Cycle Symposium, Boulder, CO, May 24-25.

Moisseytsev, A. and Sienicki, J. J., 2012, “Modeling of the SNL S-CO_2 Loop with ANL Plant Dynamics Code”, Proceedings of 20th International Conference on Nuclear Engineering, ICONE-20, Anaheim, CA, July 30 – August 3.

Moisseytsev, A. and Sienicki, J. J., 2013, “Validation of the ANL Plant Dynamics Code with the SNL S-CO_2 Loop Transient Data,” GT2013-94893, Proceedings of ASME Turbo Expo 2013, GT2013, San Antonio, Texas, USA, June 3-7.

Span, R. and Wagner,W., 1996, “A New Equation of State for Carbon Dioxide Covering the Fluid Region From the Triple-Point Temperature to 1100 K at Pressures up to 800 MPA,” Journal of Physical and Chemical Reference, vol. 25, no. 6, pp. 1509–1596.

Vilim, R. B. and Moisseytsev, A., 2008, “Comparative Analysis of Supercritical CO_2 Power Conversion System Control Schemes,” Paper 8372, 2008 International Congress on Advances in Nuclear Power Plants (ICAPP 2008), Anaheim, CA, June 8-13.

ACKNOWLEDGEMENTS

Argonne National Laboratory’s work was supported by the U. S. Department of Energy Advanced Reactor Concepts (ARC) and Advanced Small Modular Reactor (aSMR) Program under Prime Contract No. DE-AC02-06CH11357 between the U.S. Department of Energy and UChicago Argonne, LLC.. The authors are grateful to Gary Rochau (SNL), the Technical Area Lead, Bob Hill (ANL/NE), the National Technical Director, and Brian Robinson, the Headquarters Program Manager for the aSMR and ARC Programs. The authors appreciate the efforts of Tom Conboy and Jim Pasch (SNL) in transferring data to ANL and explaining the experiment data and operational procedures.